Magnetic flux pinning in superconductors with hyperbolic-tessellation arrays of pinning sites

V. R. Misko[1,2] and Franco Nori[1,3]

[1]*Advanced Science Institute, RIKEN, Wako-shi, Saitama 351-0198, Japan*

[2]*Departement Fysica, Universiteit Antwerpen, B-2020 Antwerpen, Belgium*

[3]*Physics Department, University of Michigan, Ann Arbor, Michigan 48109-1040, USA*

(Received 1 November 2011; revised manuscript received 16 April 2012; published 4 May 2012; publisher error corrected 8 June 2012)

We study magnetic flux interacting with arrays of pinning sites (APSs) placed on vertices of hyperbolic tessellations (HTs). We show that, due to the gradient in the density of pinning sites, HT APSs are capable of trapping vortices for a broad range of applied magnetic fluxes. Thus, the penetration of magnetic field in HT APSs is essentially different from the usual scenario predicted by the Bean model. We demonstrate that, due to the enhanced asymmetry of the surface barrier for vortex entry and exit, this HT APS could be used as a "capacitor" to store magnetic flux.

DOI: 10.1103/PhysRevB.85.184506 PACS number(s): 74.25.Wx, 02.40.−k, 74.25.Uv, 74.78.Na

I. INTRODUCTION

Non-Euclidean geometries have had a very profound effect in physics,[1] not only in general relativity, but also more recently in condensed-matter physics.[2–4] Some examples include order and defects in liquids and metallic glasses,[5] polytope models of glass[6] in a curved icosahedral space, icosahedral bond-orientational order in supercooled liquids,[7] etc. Recently, topological defects, i.e., disclinations, dislocations, and vortices, were studied on rigid substrates of spatially varying Gaussian curvature.[8] Here we present a study on vortex pinning in hyperbolic two-dimensional (2D) tessellations.

In mesoscopic superconductors, the geometry of a sample and/or its underlying pinning has a strong impact on its vortex pattern, for example, the appearance of vortex concentric "shells"[9–11] in mesoscopic disks, which can even merge into so-called giant vortices[12] in very small disks. In symmetric polygons, e.g., triangles and squares, vortices tend to form patterns with the symmetry of the polygon boundary. Moreover, the sample symmetry can even lead to a spontaneous generation of antivortices to restore the broken symmetry for incommensurate magnetic flux.[13,14] Furthermore, vortex patterns can also be produced by various arrays of pinning sites (APSs) (see, e.g., Ref. 15). Even for the simplest case of a square APS, a variety of patterns and phases were found.[16]

Using APSs incommensurate with vortex lattices results in an elastic deformation of the vortex lattice and thus in an increase in the elastic energy. However, pinning properties of a superconductor can be even improved by using incommensurate APS sites, as recently demonstrated (theoretically[17,18] and experimentally[19–22]) for quasiperiodic (QP) tiling APSs. The important property of QP APSs[17–22] is the existence of many built-in periods resulting in flux pinning for various flux densities. This unique property, in turn, opens the possibility for the design of fluxonics devices with enhanced pinning over a broad range of fields.

In this paper, we investigate pinning properties of a superconductor with pinning sites placed on the vertices of a *hyperbolic tessellation* (HT). One important property which makes this system different from the family of QP tilings, is that a HT (i.e., its projection from hyperbolic to a 2D Euclidean space, e.g., in a Poincaré disk representation) is a finite-size system. This makes HT somewhat similar to mesoscopic symmetric experimental samples,[9,10,12,13] although with additional internal structure and less rigid "boundaries." We show that a HT APS exhibits an enhanced asymmetry of its surface barrier, for vortex entry and expulsion.

Hyperbolic tessellations are obtained as a projection of a tiling of regular symmetric polygons in a hyperbolic space to a two-dimensional Euclidean space. (Similarly, QP tilings are obtained as a 2D projection of tilings which are periodic in a higher dimensional space.) As a result, a 2D HT is a set of topologically equivalent tilings of decreasing sizes (from the center and toward the edge) which makes this system attractive for pinning magnetic flux, as we demonstrate below. Each tessellation is represented by a Schläfli symbol of the form $\{p,q\}$, which means that q regular p-gons surround each vertex. There exists a hyperbolic tessellation $\{p,q\}$ for every p,q such that $(p-2)(q-2) > 4$.[1–3,5,6] Note that the ones based on a regular $\{p,q\}$ are the same as the dual ones based on a regular $\{q,p\}$, but shown in a different orientation (see Fig. 1).

II. SIMULATION

We model a three-dimensional (3D) column, infinitely long in the z direction, by a 2D (in the xy plane) square simulation cell (see Fig. 2) with periodic boundary conditions. The free-of-pinning region between the HT APS and the boundary of the simulation cell serves as a reservoir of vortices that mimics the externally applied magnetic field. This approach has been successfully used in numerous simulations in the past (see, e.g., Refs. 17, 18, 21, and 23–25). To study the dynamics of vortex motion, we numerically integrate the overdamped equations of motion (see, e.g., Refs. 17 and 18):

$$\eta \mathbf{v}_i = \mathbf{f}_i = \mathbf{f}_i^{vv} + \mathbf{f}_i^{vp} + \mathbf{f}_i^{T} + \mathbf{f}_i^{d}. \quad (1)$$

Here $\mathbf{f}_i$ is the total force per unit length acting on vortex i, $\mathbf{f}_i^{vv}$ and $\mathbf{f}_i^{vp}$ are the forces due to vortex-vortex and vortex-pin interactions, respectively, $\mathbf{f}_i^{T}$ is the thermal stochastic force, and $\mathbf{f}_i^{d}$ is the driving force; $\mathbf{v}_i$ is the velocity, and η is the viscosity. All the forces are expressed in units of $f_0 = \Phi_0^2/8\pi^2\lambda^3$, where $\Phi_0 = hc/2e$, and lengths (fields) in units of λ (Φ_0/λ^2).

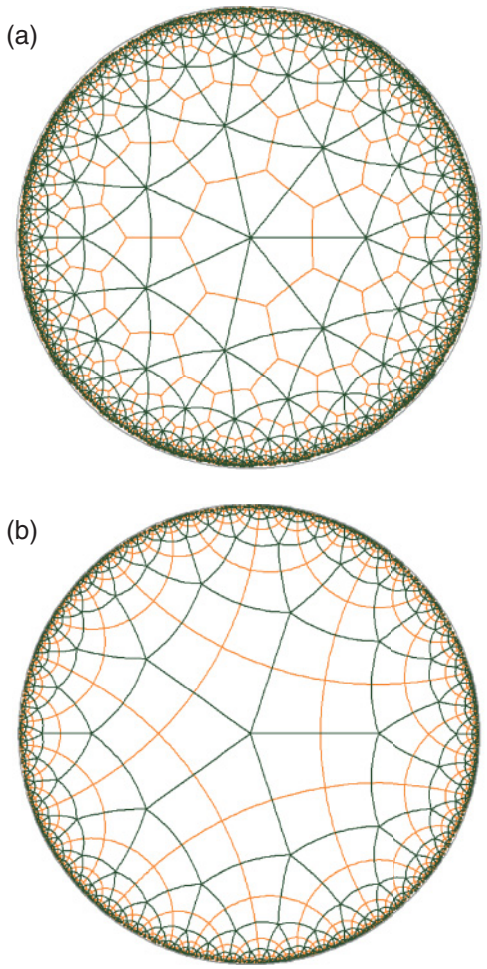

FIG. 1. (Color online) Hyperbolic tessellations in a Poincaré disk. The Shchläfli symbols $\{p,q\}$ describe tessellations where q regular p-gons meet at each vertex: (a) {3,7} and (b) {4,5} (shown by dark green/black lines). The corresponding dual tessellations (a) {7,3} and (b) {5,4} are shown by orange (gray in black and white) lines.

Following Refs. 17, 18, 21, and 23–25, the force due to the interaction of the ith vortex with other vortices is

$$\mathbf{f}_i^{vv} = \sum_j^{N_v} f_0 K_1\left(\frac{|\mathbf{r}_i - \mathbf{r}_j|}{\lambda}\right)\hat{\mathbf{r}}_{ij}, \tag{2}$$

where N_v is the number of vortices, and K_1 is a first-order modified Bessel function.

Vortex pinning is modeled by short-range parabolic potential wells located at positions $\mathbf{r}_k^{(p)}$. The pinning force is

$$\mathbf{f}_i^{vp} = \sum_k^{N_p}\left(\frac{f_p}{r_p}\right)|\mathbf{r}_i - \mathbf{r}_k^{(p)}|\Theta\left(\frac{r_p - |\mathbf{r}_i - \mathbf{r}_k^{(p)}|}{\lambda}\right)\hat{\mathbf{r}}_{ik}^{(p)}, \tag{3}$$

where N_p is the number of pinning sites, f_p is the maximum pinning force of each potential well, r_p is the range of the pinning potential, Θ is the Heaviside step function, and $\hat{\mathbf{r}}_{ik}^{(p)} = (\mathbf{r}_i - \mathbf{r}_k^{(p)})/|\mathbf{r}_i - \mathbf{r}_k^{(p)}|$.

The temperature contribution $\mathbf{f}_i^T$ is represented by a stochastic term obeying the following conditions:

$$\langle f_i^T(t)\rangle = 0 \tag{4}$$

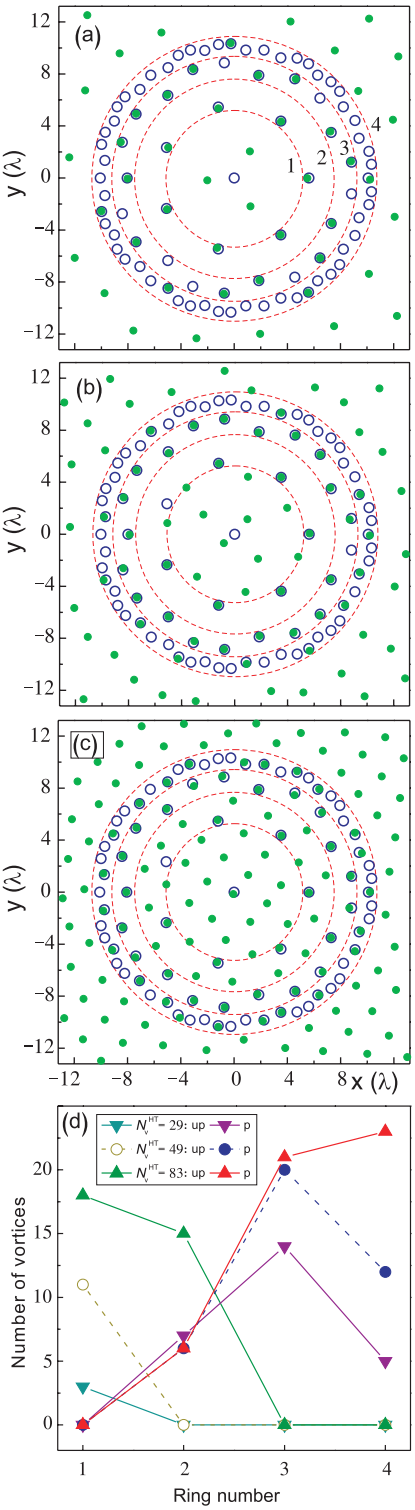

FIG. 2. (Color online) Vortex configurations in a {3,7} hyperbolic-tessellation (HT) APS for varying number of vortices per simulation cell (inside the HT): (a) $N_v = 49$ ($N_v^{\mathrm{HT}} = 29$), (b) $N_v = 81$ ($N_v^{\mathrm{HT}} = 49$), and (c) $N_v = 144$ ($N_v^{\mathrm{HT}} = 83$). Pinning sites are shown by dark blue (black) open circles, vortices by green (gray) dots. Red (gray) dashed lines show the boundaries of concentric rings [numbered 1 to 4 (a)] of the same area containing 1, 7, 21, and 56 pins. (d) Number of pinned (p) and unpinned (up) vortices in the rings, corresponding to N_v^{HT} in (a)–(c), shown by symbols (lines connecting the symbols are guides for the eye).

and

$$\left\langle f_i^T(t) f_j^T(t') \right\rangle = 2\eta k_B T \delta_{ij}\, \delta(t - t'). \quad (5)$$

To obtain the ground state of a system of vortices, the system starts at some nonzero value of the "temperature" and gradually decrease it to zero, i.e., we perform a simulated-annealing simulation. This procedure mimics the annealing procedure in field-cooled experiments. This method was employed for the calculations of equilibrium vortex configurations to study the pinning properties of the HT APSs.

For the simulation of flux entry, vortices were instead injected in the simulation region, at random positions at its boundary, thus mimicking an increasing external field. Correspondingly, flux expulsion was simulated by the random removal of vortices from the region outside the HT, mimicking a decreasing external field. These simulations were performed at zero temperature.

III. VORTEX CONFIGURATIONS IN A HYPERBOLIC-TESSELLATION APS

Let us consider vortices on a HT APS. One might naively expect that, in order to pin all the vortices, the ideal pinning potential should be a sixfold symmetric HT {3,6}. This tessellation is composed of triangles, such that six triangles join each vertex, as in usual Abrikosov lattices. However, configuration {3,6} does not satisfy the condition $(p-2)(q-2) > 4$ and thus such a HT does not exist.

The so-called Omnitruncated tessellation {3,7} is the "most nearly planar" of all semiregular or regular hyperbolic tessellations, in the sense that if one tried to construct it from Euclidean planar polygons, the sum of the angles at each vertex would be as small as possible, while exceeding 360°. Therefore, we choose the {3,7} HT for our numerical simulations (although other HT will possess similar pinning properties).

Figure 2 shows simulated stable vortex configurations in a {3,7} HT APS for various values of the applied magnetic flux. As shown in Fig. 2(a), for low vortex densities (e.g., for $N_v =$ 49 vortices per simulation cell), vortices are mainly pinned by the central region of the HT. For higher densities (e.g., $N_v = 81$), vortices are pinned by the central and intermediate region Fig. 2(b). Finally, for an even higher vortex density (e.g., $N_v = 144$), the vortex lattice is commensurate with the pinning centers near the boundary, and therefore are more efficiently pinned in that region [Fig. 2(c)].

To analyze this observation in a more quantitative way, we divide the entire area of the HT in concentric rings of equal areas [Fig. 2(a)]. These rings of increasing radius contain 1, 7, 21, and 56 pinning sites, correspondingly (hereafter, we ignore the central pinning site, assuming that the mobility of the vortices can be examined by rotating them with respect to the center of the HT, which can be experimentally realized in a Corbino setup—see, e.g., Refs. 26–28). For the numbers of vortices considered here inside the HT (i.e., $N_v^{\mathrm{HT}} = 29$, 49, and 83), the inner region contains 3, 11, and 18 unpinned vortices, correspondingly. The first inner ring accommodates, respectively, 7, 6, and 6 pinned plus 15 unpinned vortices, i.e., all the vortices in case of low densities ($N_v^{\mathrm{HT}} = 29$ and 49) in this central ring turn out to be pinned, while for the higher density, i.e., $N_v^{\mathrm{HT}} = 83$, this ring is less efficient in terms of its pinning properties. The third ring, which is characterized by a higher density of pinning sites, is efficient for all the vortex densities considered, and it is able to trap more vortices with increasing vortex density. However, for the highest vortex density ($N_v^{\mathrm{HT}} = 83$), most of the pinned vortices are pinned by the outer ring. These results are summarized in Fig. 2(d).

The mobility of vortex matter pinned by the HT APS can be examined, e.g., by applying a Corbino-type radially decreasing external current (which, in addition, produces a shear stress) or simply by applying temperature. Thus, for low temperatures (and low vortex densities), the following holds: The vortices at or near the center will be in a *liquid* state, as they are not pinned and can freely move; the vortices further away from the center will be in a *viscous liquid* vortex state, as they are only partially pinned (e.g., the vortices in the third ring for $N_v^{\mathrm{HT}} = 83$); and the vortices located near the edges will be in a *solid* phase, because there are many pinning sites near the edges. Therefore, a single sample could exhibit three different vortex phases.

IV. MAGNETIC FLUX PENETRATION IN A HT APS

Due to the gradient in the density of pinning sites (which resulted, as shown above, in strongly inhomogeneous pinning of vortices), the penetration of magnetic flux in a HT APS is strongly inhomogeneous. The HT outer boundary has a high density of pinning sites (note that when approaching the boundary of a mathematical HT, the number of tiles and therefore the number of vertices goes to infinity, leading to an infinite density of pinning sites at the surface of the sample; however, here we consider a more realistic case of a finite number of vertices or pinning sites). The high-density-of-pins sample boundary shields the inner part of the HT APS by pinning vortices at the edge, thus preventing the magnetic flux from penetrating the HT.

Figure 3 shows the penetration of magnetic flux into a HT APS for a number of vortices varying from $N_v = 28$ [Fig. 3(a)] to 125 [Fig. 3(d)]. The initial state is prepared by annealing the vortices outside the HT such that they are homogeneously distributed in the region without pinning. After reaching a stable vortex configuration outside the "sample" (which mimics a homogeneous externally applied magnetic field), temperature is set to zero and vortices are allowed to freely move, e.g., enter the HT APS.[23] For low densities of the applied magnetic flux, i.e., ranging from $N_v = 28$ to 63 [Figs. 3(a) and 3(b)], vortices are trapped by the dense pinning sites at the boundary. With increasing flux density, and thus flux "pressure," some vortices can pass over the first pinning row but are still not able to enter the inner region of the HT, being pinned by the second row of pinning sites [Fig. 3(c) for $N_v = 81$]. For higher flux densities, magnetic flux starts to slowly penetrate the HT APS via jumps from the outer pinning rows to the inner, less dense, pinning rows, while the edge pins trap additional incoming vortices, until all the pinning sites are filled. For even higher flux densities, vortices enter the central part of the sample where they self-organize in vortex patterns which are influenced by the circular boundary of the HT and the pinning sites inside the HT (in a similar way to the formation

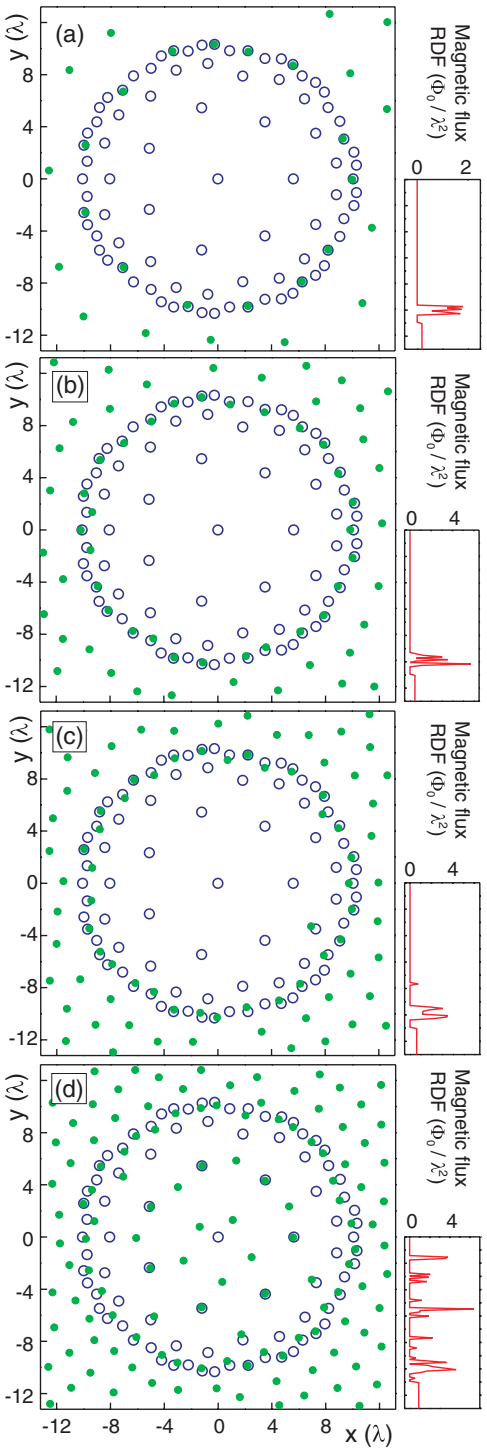

FIG. 3. (Color online) Penetration of magnetic flux in a HT APS: The ground-state vortex configurations for varying number of vortices, $N_v = 28$ (a), 63 (b), 81 (c), and 125 (d). For low and moderate applied fluxes [(a), (b)], the penetration of the magnetic flux in the HT is shielded by the outer row (i.e., at the edge) of the HT, while for higher applied fluxes [(c), (d)], vortices jump into the inner pinning sites, i.e., at the second pinning "row" and the pins at the central region, although vortices are still pinned by the outer pins. This scenario results in a very inhomogeneous magnetic flux penetration in the HT APS. The corresponding radial distribution function (RDF) of the magnetic flux penetrating in the HT APS is shown on the right-hand side panel for each N_v.

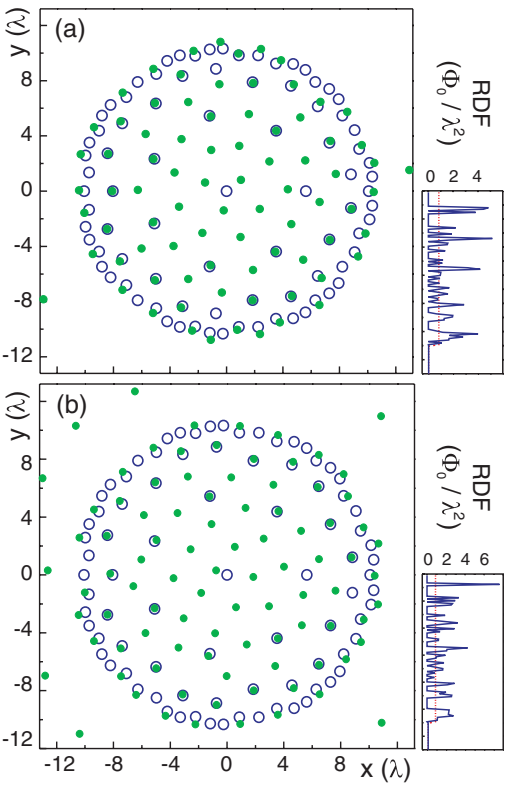

FIG. 4. (Color online) Accumulation of the magnetic flux in a HT APS and its expulsion: Vortex patterns for $N_v = 81$ (a) and 93 (b). The right-hand side panels show the corresponding RDF for the magnetic flux inside ($r/\lambda \lesssim 11$) and outside ($r/\lambda \gtrsim 11$) the HT [solid dark blue (black) line] and the average magnetic flux inside the HT [dashed red (gray) line].

of vortex "shells" in mesoscopic superconducting disks with strong pinning[10]).

The profile of the magnetic flux entering the HT APS as a function of the distance from the center of the HT, i.e., the radial distribution function (RDF), is shown in Figs. 3(e)–3(h). The flux is accumulated in the vicinity of the sample boundary for moderate applied magnetic fluxes, and it penetrates deep inside the sample for larger fluxes. This scenario is in a sharp contrast to the conventional flux penetration described by the Bean model.

V. FLUX EXPULSION AND ACCUMULATION

Another interesting property of the HT APS is the asymmetry of the sample boundary, i.e., inside and outside the HT. Of course, trapped flux in usual samples with no pinning is enhanced by the Bean-Livingston barrier.[29] Adding pinning sites near the edges (as in a HT APS) strongly enhances this effect.

To simulate flux expulsion and accumulation, the initial state is prepared by annealing the vortices *inside* the HT. After reaching a stable vortex configuration inside the HT, temperature is set to zero and vortices are allowed to move freely, i.e., they can leave the "sample" if the vortex density is sufficient. Magnetic flux accumulation in a HT APS and its expulsion is illustrated in Fig. 4.

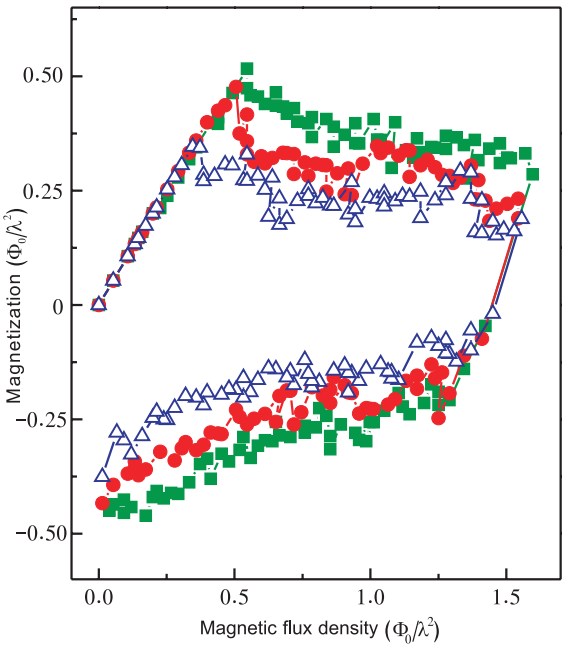

FIG. 5. (Color online) Magnetization curves for the HT APS with varying maximum pinning strength: $f_p/f_0 = 1.2$ (squares), 1 (circles), and 0.8 (open triangles).

We analyzed the critical values for entry and expulsion of the magnetic flux and found that it is higher for the flux expulsion. For example, for a HT array of narrow pinning sites characterized by the maximum pinning force $f_p/f_0 = 2$ and radius $r_p/\lambda = 0.3$, the ratio of the critical magnetic flux for flux expulsion to that of flux entry is $\Phi_{\text{out}}/\Phi_{\text{in}} \approx 1.27$. This enhanced asymmetry in flux entry and expulsion might be useful for potential applications of HT APS as a "capacitor"-type fluxonic device accumulating magnetic flux.

We calculated the magnetization of the sample exploiting the analogy between the vortices in the region outside the HT (i.e., free of pinning) and external field. The integrated difference between this field and the internal field[30] across the sample yields the magnetization M.[23] In our calculations of the magnetization for the ramp-up phase, the number of vortices *outside* the HT was gradually increased from zero to $N_v^{\max}$, then it was gradually decreased to zero for the ramp-down phase. Note that in this manner only a part of the magnetization loop can be calculated, i.e., for positive values of the magnetic field since the field cannot be inverted using this method.[23] Additional vortices were injected, one by one, at random positions at the boundaries of the simulation cell, providing a homogeneous distribution of the external magnetic field outside the sample.

The calculations were performed for different pinning strengths. Typical magnetization curves are shown in Fig. 5. First, the magnetization M increases linearly with the external field. It is interesting that the low-field slope of M is equal to 1, reflecting the fact that magnetic flux does *not* penetrate the sample being shielded by the external boundary, i.e., the sample displays perfect diamagnetism. After reaching the maximum, M starts to decrease due to vortices entering the sample. Note that this behavior of the magnetization in a HT APS is similar to that of a superconductor in a Meissner state. However, the magnetic flux is not "expelled" from the sample by a screening supercurrent as in usual superconductors in an external field. In a HT APS, the role of the screening current is played by the vortices which are pinned by the external row of pinning sites situated at the HT boundary. These pinned vortices repel incoming vortices and thus prevent the external flux from entering the sample. For various values of the pinning strength, the decrease in the magnetization, after reaching the maximum, can be either smooth (curves for $f_p/f_0 = 1.2$ and 0.8 in Fig. 5) or sharp ($f_p/f_0 = 1$), depending on the parameters of the HT APS. Further exploiting the similarity to the magnetization of a superconductor in an external magnetic field, one can notice that this behavior resembles the magnetization in either *type-II* or *type-I* superconductors, although the reason for this behavior here can be due to commensurability effects.

The magnetization of the HT has a remarkable hysteresis loop, as seen from the decreasing-field part of the magnetization curves in Fig. 5.

VI. CONCLUSIONS

We demonstrated that arrays of pinning sites (APSs) placed on vertices of hyperbolic tilings, or tessellations (HTs), can efficiently trap flux of different densities, in contrast to periodic APSs which are efficient for few specific matching flux values. Vortex matter in this device can coexist in three different phases, namely, in a liquid phase (near the center), in a viscous liquid vortex phase (further from the center), and in a solid phase (near the boundary). This could be considered as a vortex analog of phases of matter inside some planets: a molten matter at the core, a viscous fluid surrounding the core, and a solid crust.

We analyzed the magnetic flux entry and exit from a HT APS. For relatively low fluxes, the outer row of pinning sited shields the interior of the sample, giving rise to a strongly inhomogeneous magnetic flux penetration, in contrast to that predicted by the conventional Bean model. The magnetization of this device has a linear part (for low applied magnetic fields) with the slope equal to one, which is indicative of a perfect diamagnetism similar to that in a Meissner state of a superconductor, although in a HT APS this occurs due to the shielding effect of trapped vortices in the outer pinning ring. Due to the asymmetry in flux entry and exit, the magnetization of the HT APS displays a remarkable hysteresis.

Our predictions can be readily verified, e.g., in experiments on magnetization measurements. In particular, such measurements can be done using an array of HTs, to provide a sufficiently strong magnetization to be detected in experiments. Furthermore, our results for superconducting vortices can be easily extended to other systems of interacting particles, e.g., colloids in a HT potential landscape created by lasers. Our results are general since they do not depend on a specific form of interparticle interaction but rather reflect the more fundamental interplay between discrete periodic elastic media and incommensurate hyperbolic tilings.

ACKNOWLEDGMENTS

V.R.M. acknowledges support from the "Odysseus" Program of the Flemish Government & FWO-Vl, and the IAP. F.N. is partially supported by the ARO, NSF Grant No. 0726909, JSPS-RFBR Contract No. 12-02-92100, Grant-in-Aid for Scientific Research (S), MEXT Kakenhi on Quantum Cybernetics, and the JSPS via its FIRST program.

[1]T. Frankel, *The Geometry of Physics: An Introduction*, 2nd ed. (Cambridge University Press, Cambridge, UK, 2004).
[2]D. R. Nelson, *Defects & Geometry in Condensed Matter Physics*, 2nd ed. (Cambridge University Press, Cambridge, UK, 2002).
[3]J.-F. Sadoc and R. Mosseri, *Geometrical Frustration* (Cambridge University Press, Cambridge, UK, 1999).
[4]M. J. Bowick and L. Giomi, Adv. Phys. **58**, 449 (2009).
[5]D. R. Nelson, Phys. Rev. B **28**, 5515 (1983).
[6]D. R. Nelson and M. Widom, Nucl. Phys. B **240**, 113 (1984).
[7]P. J. Steinhardt, D. R. Nelson, and M. Ronchetti, Phys. Rev. Lett. **47**, 1297 (1981); Phys. Rev. B **28**, 784 (1983).
[8]A. M. Turner, V. Vitelli, and D. R. Nelson, Rev. Mod. Phys. **82**, 1301 (2010).
[9]I. V. Grigorieva, W. Escoffier, J. Richardson, L. Y. Vinnikov, S. Dubonos, and V. Oboznov, Phys. Rev. Lett. **96**, 077005 (2006).
[10]I. V. Grigorieva, W. Escoffier, V. R. Misko, B. J. Baelus, F. M. Peeters, L. Y. Vinnikov, and S. V. Dubonos, Phys. Rev. Lett. **99**, 147003 (2007).
[11]V. A. Schweigert, F. M. Peeters, and P. S. Deo, Phys. Rev. Lett. **81**, 2783 (1998).
[12]A. Kanda, B. J. Baelus, F. M. Peeters, K. Kadowaki, and Y. Ootuka, Phys. Rev. Lett. **93**, 257002 (2004).
[13]L. F. Chibotaru, A. Ceulemans, V. Bruyndoncx, and V. V. Moshchalkov, Nature (London) **408**, 833 (2000); Phys. Rev. Lett. **86**, 1323 (2001).
[14]V. R. Misko, V. M. Fomin, J. T. Devreese, and V. V. Moshchalkov, Phys. Rev. Lett. **90**, 147003 (2003).
[15]M. F. Laguna, C. A. Balseiro, D. Domínguez, and F. Nori, Phys. Rev. B **64**, 104505 (2001).
[16]W. V. Pogosov, V. R. Misko, H. J. Zhao, and F. M. Peeters, Phys. Rev. B **79**, 014504 (2009).
[17]V. Misko, S. Savel'ev, and F. Nori, Phys. Rev. Lett. **95**, 177007 (2005).
[18]V. R. Misko, S. Savel'ev, and F. Nori, Phys. Rev. B **74**, 024522 (2006).
[19]R. B. G. Kramer, A. V. Silhanek, J. Van de Vondel, B. Raes, and V. V. Moshchalkov, Phys. Rev. Lett. **103**, 067007 (2009).
[20]M. Kemmler, C. Gürlich, A. Sterck, H. Pöhler, M. Neuhaus, M. Siegel, R. Kleiner, and D. Koelle, Phys. Rev. Lett. **97**, 147003 (2006).
[21]V. R. Misko, D. Bothner, M. Kemmler, R. Kleiner, D. Koelle, F. M. Peeters, and F. Nori, Phys. Rev. B **82**, 184512 (2010).
[22]A. V. Silhanek, W. Gillijns, V. V. Moshchalkov, B. Y. Zhu, J. Moonens, and L. H. A. Leunissen, Appl. Phys. Lett. **89**, 152507 (2006).
[23]R. A. Richardson, O. Pla, and F. Nori, Phys. Rev. Lett. **72**, 1268 (1994).
[24]F. Nori, Science **271**, 1373 (1996).
[25]C. J. Olson, C. Reichhardt, and F. Nori, Phys. Rev. B **56**, 6175 (1997).
[26]N. S. Lin, V. R. Misko, and F. M. Peeters, Phys. Rev. Lett. **102**, 197003 (2009).
[27]S. Okuma, Y. Tsugawa, and A. Motohashi, Phys. Rev. B **83**, 012503 (2011).
[28]N. S. Lin, T. W. Heitmann, K. Yu, B. L. T. Plourde, and V. R. Misko, Phys. Rev. B **84**, 144511 (2011).
[29]C. P. Bean and J. D. Livingston, Phys. Rev. Lett. **12**, 14 (1964).
[30]It is clear that vortices will enter the pinning sites at the boundary for any external magnetic field. However, we are interested in flux penetrating *inside* the sample, and we define as "internal field" the field inside the HT excluding its boundary.